Steel and Composite Structures, *Vol. 56, No. 6 (2025) 475-486*
https://doi.org/10.12989/scs.2025.56.6.475

Mitigation of alkalinity and suspended fines in steel slag leachate via CO_2 pressurization

Jeehoon Ma[1a], Won Hee Lee[1b], Yong-Hoon Byun[2c] and Tae Sup Yun*[1]

[1]*School of Civil and Environmental Engineering, Yonsei University, 50, Yonsei-ro, Seodaemun-gu, Seoul, 03722, Republic of Korea*
[2]*Department of Agricultural Civil Engineering, Kyungpook National University, 80, Daehak-ro, Buk-gu, Daegu, 41566, Republic of Korea*

(Received May 26, 2025, Revised July 25, 2025, Accepted August 25, 2025)

Abstract. Basic Oxygen Furnace (BOF) steel slag, a major byproduct of the steel industry, has been widely recycled for various engineering applications. Before commercialization and reuse, steel slag undergoes an aging process that involves spraying water over the stacked slag for several months in open yards to mitigate the unforeseen environmental risk. This study experimentally investigates the behavior of steel slag upon exposure to water, with particular focus on the characteristics of leachate, which are closely associated with the aging process. Two steel slag types were prepared: raw materials and those pressurized with CO_2 to promote carbonate formation via reaction with Ca^{2+}. Both were packed into the column and leached with either distilled water or seawater at different flow rates. Effluent pH and turbidity were monitored over time, Also, the leachates were stirred in ambient air to allow further carbonation. Solid residues were analyzed using Scanning Electron Microscope (SEM), X-ray Energy-Dispersive Spectroscopy (EDS), and Thermogravimetric Analysis (TGA). Pressurizing steel slag with CO_2 was found to reduce leachate pH, while turbidity was primarily attributed to suspended carbonate particles. Flow rate had a negligible effect, whereas seawater interaction induced a turbidity rise.

Keywords: BOF steel slag; Alkalinity; Turbidity; CO_2 pressurized carbonation

1. Introduction

Steel slag is a byproduct generated during the steelmaking process, particularly during the production of molten steel. It can be broadly categorized into several types based on the process and stage of production, including Basic Oxygen Furnace (BOF) slag, Electric Arc Furnace (EAF) slag, and Ladle Furnace (LF) slag (Baalamurugan *et al*. 2024).

Over the past decade, the global steel slag production has increased in parallel with the growth in steel production. For example, in 2020, the worldwide generation of steel slag was estimated at approximately 180 to 270 million tons, increasing to around 190 to 290 million tons by 2024 (US Geological Survey 2025). In South Korea, about 71.8% of steel slag is currently recycled as aggregate for road construction and embankment fills, and 5.2% is reused as a raw material for cement production. Similarly, in Europe, approximately 70.6% is utilized as road aggregate and 4.5% is reused as fertilizer (Korea Iron & Steel Association 2024, Euroslag 2018).

As steel slag generation continues to rise, its importance as a reusable resource is also growing, prompting a wide range of research efforts. In particular, studies on the high-value reuse of steel slag for remediation of heavy metal-contaminated soils and water (O'Connor *et al*. 2021, Wang *et al*. 2023), as well as the production of advanced functional materials (Wang *et al*. 2013, Wang *et al*. 2018), have gained momentum in recent years. Nevertheless, despite these advancements, it is noteworthy that approximately 70% of steel slag is still directly applied to land as recycled construction aggregate. It highlights the need for more in-depth characterization of steel slag rather than limiting its use to fill applications.

Before being transported from steelworks for recycling purposes, steel slag is typically subjected to an aging treatment process. This process is most commonly conducted through water sprinkling and natural air exposure, requiring at least six months to reach an acceptable level of stabilization (Engström *et al*. 2013, Liu *et al*. 2024). However, in light of increasing slag production, the spatial limitations of aging yards and the extended duration of conventional treatment needs more efficient approaches.

Currently, the BOF process remains the dominant steelmaking method, resulting in a significantly greater production of BOF slag—approximately three times more than EAF slag and ten times more than LF slag (Korea Iron & Steel Association, 2024). Accordingly, this study focuses on the characterization and treatment of BOF steel slag.

BOF steel slag is generated as a byproduct during the oxidation of impurities in hot metal in the basic oxygen furnace process. Impurities such as phosphorus (P), carbon (C), silicon (Si), and manganese (Mn) are oxidized and removed with the assistance of added flux materials such as quicklime (CaO) and iron ore (FeO). As a result, BOF slag

*Corresponding author, Ph.D. Professor
E-mail: taesup@yonsei.ac.kr
[a]Ph.D. Student
[b]M.S. Student
[c]Associate Professor

ISSN: 1229-9367 (Print), 1598-6233 (Online)

typically contains high concentrations of ferric oxide (Fe_2O_3) and calcium-based compounds. Calcium exists in various reactive forms, including free-CaO, hydrated $Ca(OH)_2$, and dicalcium silicate (C_2S). When exposed to water, these compounds readily dissolve and release OH^- ions, resulting in a highly alkaline leachate. Furthermore, when the leachate is exposed to atmospheric CO_2, the dissolved Ca^{2+} ions react to form $CaCO_3$, which precipitates as suspended fines. This leads to turbidity in the leachate, along with secondary reactions that contribute to environmental concerns. These chemical reactions indicate that aging is not only required for physical stabilization but also plays a critical role in mitigating chemical reactions that cause high pH and turbidity. Understanding these mechanisms is essential for designing effective mitigation strategies.

Accordingly, this study aims to provide a comprehensive characterization of the leaching properties of BOF steel slag and propose a mitigation strategy based on its physicochemical response to water and atmospheric CO_2 exposure. Rather than focusing on accelerating the aging process per se, the goal is to identify how key variables, such as infiltrating liquid type and the presence or absence of carbonation, affect alkalinity and suspended fines generation during leaching. For this purpose, continuous leaching tests were conducted using two types of liquids (distilled water and artificial seawater). Additionally, a CO_2 pressurized carbonation process was applied to examine the effect of pre-carbonation on slag fate. Characterization techniques, including X-ray Computed Tomography (CT), Scanning Electron Microscopy (SEM), Thermogravimetric Analysis (TGA), and X-Ray Fluorescence (XRF), were used to assess microstructural, mineralogical, and chemical changes of steel slag resulting from these treatments.

The proposed strategy is informed by previous studies on CO_2 capture and slag stabilization via carbonation (Huijgen and Comans 2006, Huijgen *et al*. 2005), as well as seawater-based aging approaches (Li *et al*. 2020, Pan *et al*. 2017, Zhang *et al*. 2011). By identifying the mechanisms behind leachate alkalinity and turbidity, this study provides a basis for developing more effective and environmentally responsible treatment methods for steel slag reuse.

2. Experimental studies

2.1 Materials

2.1.1 BOF steel slag

Characteristics of BOF steel slag

BOF steel slag generated by POSCO (Pohang, Korea) was used in this study. The samples were prepared by sieving to retain particles smaller than a diameter of 4.75 mm while excluding fine particles smaller than 0.075 mm. The specific gravity of the BOF steel slag was measured to be 3.3 based on ASTM D854, which falls within the typical range reported for steel slag materials (Moon *et al*. 2002). The minimum and maximum void ratios of the slag were determined to be 0.489 and 0.806, respectively, using ASTM D4253 and ASTM D4254 procedures.

Table 1 Chemical compositions of BOF steel slag before CO_2 pressurization by XRF analysis

Compositions	Weight portion [wt%]
Fe_2O_3	42.47
CaO	27.45
SiO_2	15.97
MnO	3.86
MgO	3.92
Al_2O_3	2.86
Total	96.53

The chemical compositions of the raw BOF steel slag before carbonation were analyzed using XRF spectroscopy, and the results are summarized in Table 1. The analysis revealed that Fe_2O_3 and CaO were the major components, together occupying 69.9 wt% of the total composition. Minor amounts of metallic oxides such as MnO, MgO, and Al_2O_3 were also detected. The high CaO content of the slag provides favorable conditions for carbonation reactions. In steel slag, CaO exists either as free CaO, which directly reacts with CO_2 to form $CaCO_3$, or as C_2S ($CaSiO_3$), which releases Ca^{2+} ions into water. These Ca^{2+} ions subsequently react with carbonate ions (CO_3^{2-}) generated from dissolved CO_2 to form $CaCO_3$, as illustrated in Eqs. (1)-(4).

$$CaO(s) + CO_2(g/l) \rightarrow CaCO_3(s) \quad (1)$$

$$CO_2(g) + H_2O(l) \rightarrow H_2CO_3 \rightarrow 2H^+(aq) + CO_3^{2-}(aq) \quad (2)$$

$$CaSiO_3(s) + 2H^+(aq) \rightarrow Ca^{2+}(aq) + SiO_2(s) + H_2O(l) \quad (3)$$

$$CO_3^{2-}(aq) + Ca^{2+}(aq) \rightarrow CaCO_3(s) \quad (4)$$

CO_2 pressurized carbonation of BOF steel slag

CO_2 pressurized carbonation was performed to compare the effects of carbonation of BOF steel slag on the alkalinity and turbidity of leachate. The high-pressure system was designed to perform carbonation reactions by pressurizing CO_2 into the BOF steel slag (Fig. 1). CO_2 was supplied from a gas cylinder to two syringe pumps (MODEL 500D, Teledyne ISCO) connected in series, and then distributed to two high-pressure cells connected in parallel. The CO_2 pressure was controlled by operating the syringe pumps through a pressure controller, while the reaction temperature was regulated using heating jackets connected to a temperature controller. The temperature controller displayed in Fig. 1 shows four red digits, representing real-time monitoring data. The two values on the left correspond to the left pressure cell, and the two on the right to the right cell. In each pair, the upper value shows the internal temperature of the cell, while the lower value indicates the temperature of the external heating source. The device operates by adjusting the external heat in real-time to maintain the target internal temperature within each

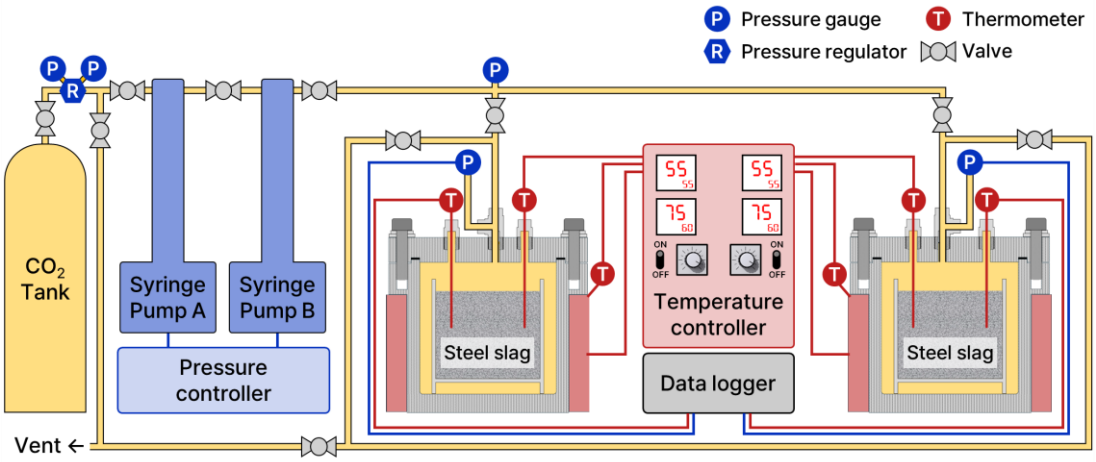

Fig. 1 CO_2 pressurized carbonation equipment using syringe pumps and the temperature controller

pressure cell. Inside the cells, pressure and temperature were monitored at 5-second intervals using a pressure gauge (PX309-2KG5V, OMEGA) and thermometers connected to a data logger (34972A, Agilent). The high-pressure cells were fabricated using SUS316L stainless steel with a wall thickness greater than 10 mm to withstand the supercritical CO_2 conditions employed in this study (55°C and 10 MPa). PTFE O-rings were installed between the cell bodies and flanges to prevent CO_2 leakage.

The wetting condition of the BOF steel slag during carbonation was designed to closely simulate industrial-scale processes. The steel slag was first saturated with distilled water, then drained and placed in a mesh bag to remove excess water. Following this procedure, the water content of the steel slag was measured to be approximately 17%. To minimize non-uniform temperature distribution caused by direct heating from the cell walls, the wetted slag was placed in a sample holder (90 mm in diameter and 80 mm in height) and then inserted into the high-pressure cell. After sealing the high-pressure system, the cells were heated using the temperature control system. Once the temperature at the center of the slag sample reached 55 °C, CO_2 was injected at a pressure of 10 MPa (i.e., supercritical state), and the carbonation reaction was maintained for 24 hours.

2.1.2 Injecting fluids in continuous leaching test

Two types of fluid were used in the leaching experiments: distilled water and synthetic seawater. The seawater was prepared by adding sea salt (MODEL CORAL PRO SALT, Red Sea) to distilled water to achieve a salinity of 35 ppt, with concentrations of calcium at 465 mg/L, magnesium at 1,390 mg/L, and potassium at 415 mg/L.

2.2 Material characterization methods

2.2.1 Optical observation

SEM imaging (JEOL-7800F, JEOL Ltd.) was implemented to observe the products formed by the carbonation process. Energy-Dispersive X-ray Spectroscopy (EDS) (JEOL-7800F, JEOL Ltd.) was employed alongside SEM imaging to complement the mineralogical analysis and verify the identity of the reaction products formed during CO_2 pressurization. These techniques enabled the direct observation of the crystal morphology, size, and distribution patterns of the precipitated materials, as well as qualitative elemental analysis (Fitzgerald and Heinrich 1968). Before SEM imaging, a thin and uniform platinum coating was applied to the sample surface using a 100-second sputter-coating process to prevent surface charging and to enhance secondary electron emission for improved image clarity. During SEM imaging, an accelerating voltage of 10.0 kV was used to scan the sample surfaces.

To investigate how carbonate precipitation alters the internal structure of BOF steel slag after CO_2 pressurized carbonation, X-ray CT scanning was performed on CO_2 pressurized BOF steel slag. The primary objective of this analysis was to visualize the spatial distribution of newly formed $CaCO_3$ and assess its potential influence on pore structure. The slag sample was prepared under the same wetting and reaction conditions (temperature and pressure) as those used in the main carbonation experiments, and placed inside a borosilicate vial with an inner diameter of 12.5 mm. The X-ray CT scanning was carried out using a TVX-IMT300CT system (Techvalley Co., Korea) with constant operating parameters: 70 kV X-ray source voltage, 400 μA current, 3 frames per second rotation speed, and a total of 4,000 projections collected over a 23-minute scan duration. The resulting CT images were reconstructed with an isotropic voxel resolution of 8.83 μm in both width and height.

2.2.2 Quantitative analysis

Thermogravimetric Analysis (TGA) was conducted to quantitatively assess the amount of $CaCO_3$ formed through the carbonation of the steel slag. This method utilizes the characteristic thermal decomposition behavior of $CaCO_3$ within a specific temperature range to estimate its content (Coats and Redfern 1963, Garlan *et al.* 2013). TGA measurements were performed on the steel slag samples before and after carbonation using an SDT 500 instrument (TA Instruments). The temperature was increased in the range of 300-900°C at a heating rate of 10 °C/min, and the

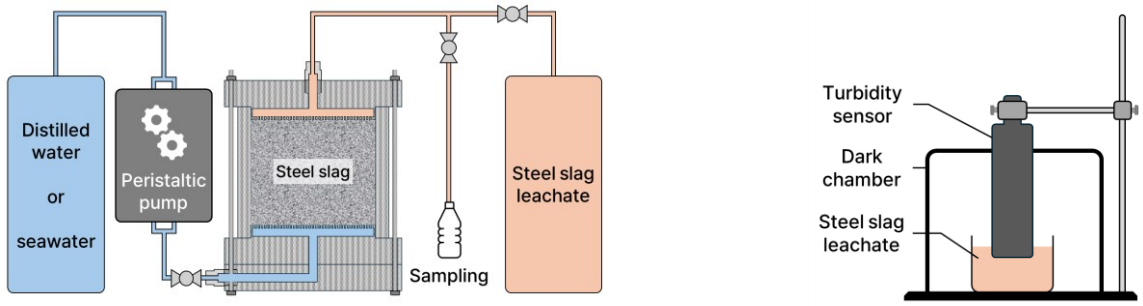

(a) Leaching test equipment using a peristaltic pump (b) Turbidity measurement system

Fig. 2 Schematic diagrams of steel slag leaching test equipment using a peristaltic pump and a turbidity measurement system

instrument's balance sensitivity was 0.1 μg. To minimize additional reactions with atmospheric CO_2 during the TGA process, the measurements were conducted under an N_2 atmosphere gas condition.

2.3 Experiment procedure

A series of continuous leaching tests was conducted to understand the characteristics of BOF steel slag leachate. The variables considered in the experiments included the CO_2 pressurized carbonation status of the BOF steel slag, the types of injecting fluid (distilled water or synthetic seawater), and the flow rate. The effects of each variable on the alkalinity and turbidity of the leachate were systematically analyzed. The case IDs and corresponding experimental conditions are summarized in Table 2.

The experimental system for the continuous leaching tests of BOF steel slag is presented in Fig. 2(a). The test column was designed with a diameter of 95 mm and a height of 80 mm. pH was measured using a probe (SevenDirect SD23, METTLER TOLEDO) with a resolution of ±0.002. Turbidity measurements were carried out as shown in Fig. 2(b). To prevent optical noise from ambient light, measurements were taken in a dark chamber. The turbidity sensor (PTU-8011, STARKO INSTRUMENTS) was mounted securely using a stand and clamp to avoid movement during measurement. The sensor probe was consistently immersed 20 mm above the bottom of the beaker to minimize potential measurement errors.

The BOF steel slag was compacted within the column to achieve a relative density of approximately 60%, reflecting typical embankment fill conditions. Two types of fluid were injected into the test column fully packed with saturated BOF steel slag, at controlled flow rates, until 100 Pore Volumes (PV, 1 PV = 216 mL) had passed through the specimen. Two flow rate cases were adopted: 36 mL/min and 72 mL/min. The flow rate for the continuous leaching test was determined based on a hypothetical field scenario where BOF steel slag is used as unpaved embankment fill. Specifically, the estimation was grounded on an extreme rainfall intensity of 60.6 mm/hr derived from local climate data (Ministry of Land, Infrastructure, and Transport 2011). Given the unpaved condition, it was assumed that 85% of the rainfall would infiltrate into the ground. An equivalent flow of 35.02 mL/min per 1.15 kg of slag was applied the site-specific parameters, a slag application volume of 105,375 tons and a surface area of 373,477 m^2, the infiltration rate was scaled down to laboratory conditions. As the pore volume of the test column was approximately 216 mL under the target compaction density, the low flow rate was rounded to 36 mL/min for ease of implementation. In support of this setup, a constant head permeability test was conducted using BOF steel slag compacted to a relative density of 60%, resulting in a hydraulic conductivity of 0.031 cm/s. This validated the feasibility of the selected flow rate ranges under typical field compaction conditions. In addition, a higher flow rate of 72 mL/min was adopted to investigate how flow rate variation influences leachate turbidity and pH. This higher condition was intended to simulate scenarios where artificial irrigation or water spraying might occur during field aging. Since detailed irrigation rates for steel slag are not well-documented, the faster condition was conservatively set as twice the slower flow rate. The flow rate was maintained using a peristaltic pump, with the 36 mL/min case operated for 10 hours, and the 72 mL/min case for 5 hours. Leachate sampling was conducted at 10 PV intervals to monitor changes in pH and turbidity.

3. Results

3.1 CO_2 pressurized carbonation of BOF steel slag

3.1.1 Grain size distributions

The carbonation of BOF steel slag was conducted under supercritical CO_2 conditions (55 °C, 10 MPa). Fig. 3 presents the Grain Size Distributions (GSD) of the BOF steel slag before and after CO_2 pressurized carbonation. Before CO_2 pressurization, the BOF steel slag exhibited a median particle size (D_{50}) of 1.29 mm, a coefficient of uniformity (c_u) of 5.11, and a coefficient of curvature (c_c) of 1.16. After CO_2 pressurization, the D_{50} increased to 2.29 mm, with a c_u of 3.52 and a c_c of 1.14, classifying the material as well-graded sand (SW) according to the Unified Soil Classification System (USCS). The increase in the proportion of coarser particles after carbonation is attributed to the partial amalgamation of BOF steel slag particles, as emphasized in Fig. 4(a). These bonds are formed by calcium carbonate ($CaCO_3$) precipitated through the reaction with CO_2, causing smaller particles to agglomerate and behave as larger particles.

Table 2 Experimental cases of the continuous leaching test

Case IDs	Slag type		Injected fluid		Flow rate	
	RS[1)]	CS[2)]	DW[3)]	SW[4)]	Slow	Fast
RDS	○		○		○	
RDF	○		○			○
RSS	○			○	○	
RSF	○			○		○
CDS		○	○		○	
CDF		○	○			○
CSS		○		○	○	
CSF		○		○		○

RS[1)] : BOF steel slag before CO_2 pressurization
CS[2)] : BOF steel slag after CO_2 pressurization
DW[3)] : distilled water SW[4)] : seawater

3.1.2 SEM-EDS analysis

The products formed during the CO_2 pressurization process were observed using SEM scanning. Fig. 4(b) presents the SEM image of the BOF steel slag particle surface after CO_2 pressurized carbonation. The image shows that the particle surface is extensively covered with precipitates formed during the CO_2 pressurization. Due to the accelerated carbonation kinetics under supercritical conditions, the reactants tend to be crystallized as an amorphous morphology rather than forming well-defined crystalline phases such as calcite or aragonite (Blue *et al*. 2017, Ma *et al*. 2024, Nancollas and Reddy 1971). Consistent with previous findings, the precipitates observed in this study were amorphous, with few instances of rhombohedral calcite or needle-like aragonite crystals.

To verify that the precipitates formed were $CaCO_3$, EDS analyses were performed at 4 spots indicated in Fig. 4(b), and the results are summarized in Table 3. Since the $CaCO_3$ molecule consists of calcium (Ca), carbon (C), and oxygen (O) atoms in an approximate ratio of 1:1:3, an elemental analysis showing atomic percentages close to 20% Ca, 20% C, and 60% O is considered indicative of $CaCO_3$ (Spínola *et al*. 2021). Therefore, spots 1–3 corresponded to locations where $CaCO_3$ crystals had formed, while spot 4 exhibited residual CaO from the original slag and possibly some graphite components inherent in the BOF steel slag.

3.1.3 X-ray CT scanning

The formation of $CaCO_3$ within the packed BOF steel slag was observed using X-ray CT scanning. Fig. 5 presents a representative cross-sectional X-ray CT image of BOF steel slag subjected to CO_2 pressurized carbonation. Carbonate precipitates appear as darker regions relative to BOF steel slag particles, yet brighter than the voids due to the higher specific gravity of BOF steel slag (3.3) compared to $CaCO_3$ (2.7). Areas identified as $CaCO_3$ were highlighted by yellowish pseudo color for clarity. Localized precipitation of $CaCO_3$ is evident both along the surfaces of slag particles and near the inner wall of the borosilicate vial. Interparticle carbonate bridging was observed, where $CaCO_3$ filled the voids between adjacent particles,

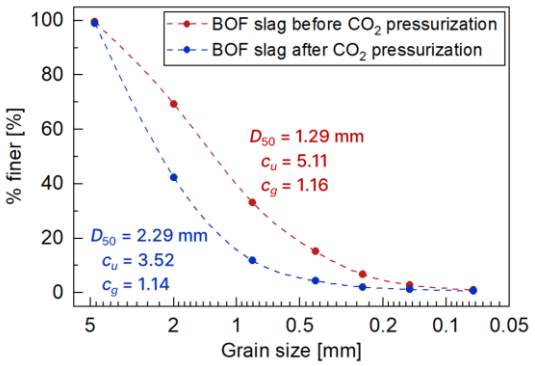

Fig. 3 Grain size distributions of BOF steel slag before and after CO_2 pressurization

Table 3 SEM-EDS result of carbonated steel slag

Spot no.	Atomic portion [%]			
	C	O	Ca	Total
1	22.55	69.90	16.55	100.00
2	25.61	61.83	12.56	100.00
3	28.60	61.81	9.59	100.00
4	11.78	41.35	46.88	100.00

suggesting a potential bonding effect that could influence the aggregate structure to corroborate Fig. 4(a).

3.1.4 Quantitative analysis of $CaCO_3$ precipitation

The amount of $CaCO_3$ precipitated before and after carbonation of the steel slag was quantified using TGA. In this analysis, the target compounds for quantification were $Ca(OH)_2$ and $CaCO_3$. $Ca(OH)_2$ thermally decomposes between 350-450 °C into CaO and H_2O, with the mass loss corresponding to the evaporation of H_2O (Eq. (5)). Similarly, $CaCO_3$ thermally decomposes above 600 °C into CaO and CO_2, with the mass loss corresponding to the release of CO_2 (Eq. (6)). The decomposition of $CaCO_3$ was evaluated within the temperature range of 600–750 °C based on the temperature–mass curves obtained from the TGA analysis (Fig. 6).

$$Ca(OH)_2(s) \rightarrow CaO(s) + H_2O(g) \quad (5)$$

$$CaCO_3(s) \rightarrow CaO(s) + CO_2(g) \quad (6)$$

For the BOF steel slag before CO_2 pressurization, a mass loss of 0.83% relative to the total sample weight was observed within the 350–450 °C range. This result indicates that the BOF steel slag contained approximately 3.41 wt% $Ca(OH)_2$, which had formed by the reaction of CaO with water or moisture before carbonation. Additionally, a mass loss of 0.48% was observed within the 600–750 °C range, corresponding to approximately 1.09 wt% $CaCO_3$, presumably formed through reaction with atmospheric CO_2 before CO_2 pressurization. For the CO_2 pressurized BOF steel slag, a mass loss of 0.38% was observed in the 350–450 °C range, while a mass loss of 5.55% was detected in the 600–750 °C range. These results indicate that after the

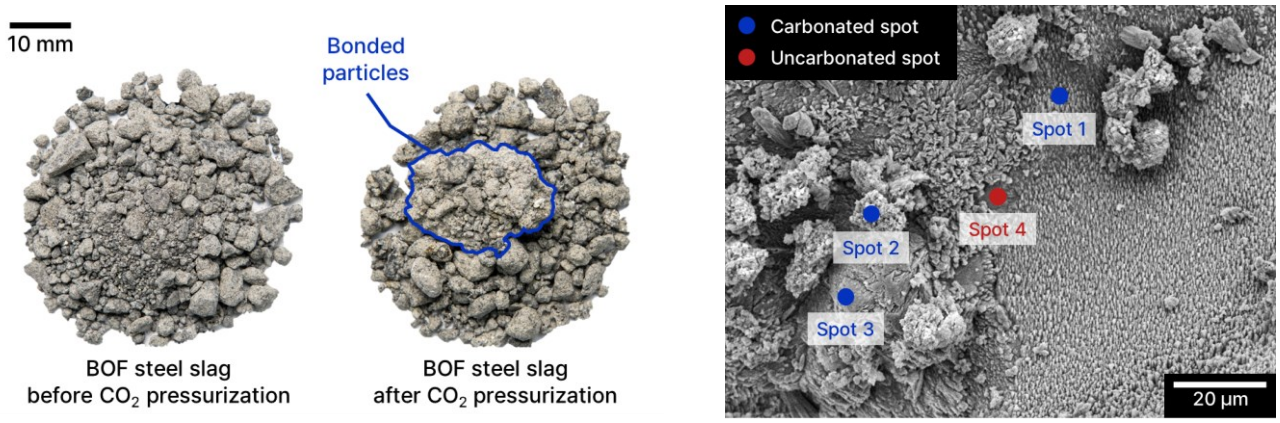

(a) Optical images of BOF steel slag before and after CO_2 pressurization

(b) Observation of $CaCO_3$ crystal by SEM imaging and EDS analysis of CO_2 pressurized steel slag

Fig. 4 Optical and SEM images of raw and CO_2 pressurized steel slag

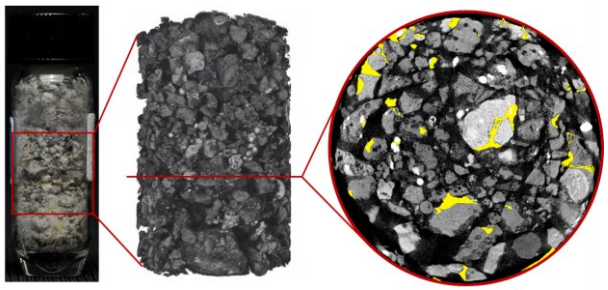

Fig. 5 Representative X-ray CT cross section of CO_2 pressurized carbonated BOF steel slag

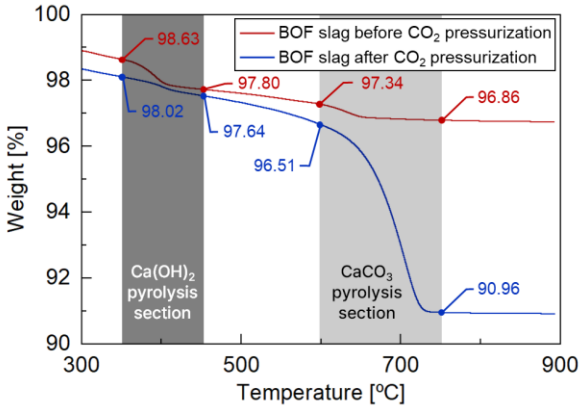

Fig. 6 Quantitative analysis of $Ca(OH)_2$ and $CaCO_3$ contents in BOF steel slag before and after CO_2 pressurization

CO_2 pressurization process, residual $Ca(OH)_2$ remained at approximately 1.56 wt% relative to the sample weight, while resultant $CaCO_3$ accounted for 12.61 wt%.

3.2 Continuous leaching test of BOF steel slag

3.2.1 Alkalinity of BOF steel slag leachate

Injected fluid volume

The pH reduction caused by ion washout with increasing injected fluid volume was found to be minor. Fig. 7(a) illustrates the change in pH during continuous leaching under a slow flow rate condition (10 PV/hr), with measurements taken at 10 PV intervals up to a total of 100 PV. In all cases, only minor changes in pH were observed as the injected fluid volume increased. When distilled water was injected through BOF steel slag before CO_2 pressurization (RDS, red solid circles with red dashed line), the pH decreased from 12.39 at 10 PV to 12.14 at 100 PV (total reduction of 0.25 over 90 PV). In the case of seawater injected to BOF steel slag before CO_2 pressurization (RSS, red solid triangles with red dashed line), the pH decreased from 10.07 at 10 PV to 9.87 at 100 PV (total change of 0.20 over 90 PV). The most notable pH reduction was observed in the CO_2 pressurized BOF steel slag injected with distilled water (CDS, blue solid circles with blue dashed line), where the pH decreased from 11.13 at 10 PV to 10.53 at 100 PV. This corresponds to a reduction of 0.60, or an average decrease rate of 6.67×10^{-3} per PV. In the case of CO_2 pressurized BOF steel slag with seawater injection (CSS, blue solid triangles with blue dashed line), the pH decreased from 8.76 to 8.54 over the same volume interval, representing a reduction of 0.22.

Fig. 7(b) presents the changes in leachate pH under a fast flow rate condition (20 PV/hr), using the same format as Fig. 7(a). The trends observed with respect to injected fluid volume, CO_2 pressurized carbonation, and injected fluid type were consistent with those under the slower flow rate. Overall, the effect of leaching volume on pH was found to be minor. The largest pH change was observed in the CO_2 pressurized BOF steel slag injected with distilled water (CDF, blue hollow circles with blue dashed line), where the pH decreased from 11.00 at 10 PV to 10.16 at 100 PV. This corresponds to a reduction of 0.84, with an average decrease rate of 9.33×10^{-3} per PV.

CO_2 pressurized carbonation status

CO_2 pressurization effectively reduced the pH of the leachate by directly removing the primary source of alkalinity in BOF steel slag. The average pH values of 10–100 PV samples in each case were compared to evaluate the effect of CO_2 pressurized carbonation status, due to the minor change in leachate pH according to the volume of injected fluid. Throughout the entire leaching period shown

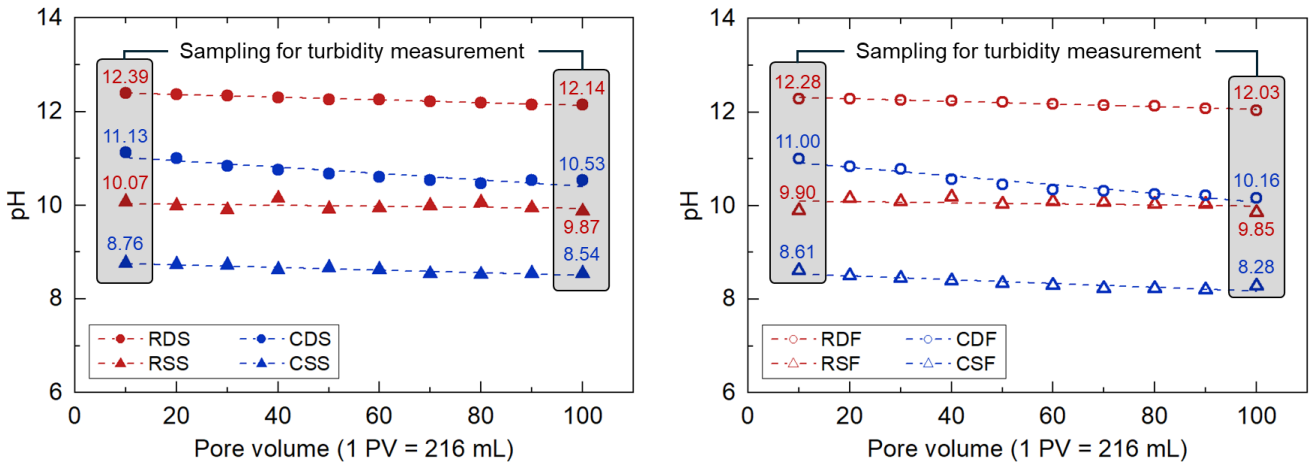

(a) Slow flow rate (10 PV/hr) conditions (b) Fast flow rate (20 PV/hr) conditions

Fig. 7 Evolution of pH value of the steel slag leachate according to seepage volume

in Fig. 7(a), the leachate pH of CDS case was 1.55 lower than the pH of the RDS case. A similar trend was observed with seawater injection, where the pH of the CSS case was 1.36 lower than the pH of the RSS case. As presented in Fig. 7(b), in distilled water injected cases, the leachate pH for CO_2 pressurized carbonated BOF steel slag (CDF) was 1.69 lower than that for the BOF steel slag before CO_2 pressurization (RDF, red hollow circles with red dashed line). For seawater injection, a difference of 1.70 was observed between CSF (blue hollow triangles with blue dashed line) and RSF (red hollow triangles with red dashed line) cases.

This reduction of alkalinity in leachate can be attributed to the mineralization of CaO into $CaCO_3$ during the CO_2 pressurized carbonation process, as CaO constitutes one of the primary alkaline components released from BOF steel slag. The reaction between CaO and CO_2 to form $CaCO_3$ is spontaneous, and $CaCO_3$ is a sparingly soluble salt under neutral to alkaline conditions (Bertos *et al*. 2004, Bychkov *et al*. 2020, Gunning *et al*. 2010, Kilic *et al*. 2016). As a result, the reverse reaction is negligible under typical leaching conditions. By stabilizing CaO as $CaCO_3$ before fluid injection, the potential for pH elevation in the leachate is significantly reduced.

Injected fluid type

The injection of seawater led to a reduction in pH, driven by reactions between seawater-derived ions and CaO present in the BOF steel slag. The average pH values of 10-100 PV samples in each case were also compared to evaluate the effect of injected fluid type. In Fig. 7(a), the leachate pH of the RSS case was 2.28 lower than the pH of the RDS case. A similar trend was observed for the carbonated slag: the average pH of the CSS case was 2.09 lower than that of the CDS case. The effect of the injecting fluid type was also consistent with the trend observed under the slower flow condition (Fig. 7(b)). Comparing the RDF case with the RSF case and the CDF case with the CSF case, the leachate pH in seawater injected cases was 2.14 and 2.15 lower, respectively.

This pH reduction is mainly attributed to the high concentration of Mg^{2+} ions in seawater. These ions react with OH^- in the leachate to form $Mg(OH)_2$ precipitates, thereby limiting the accumulation of free OH^- and suppressing excessive alkalinity. $Mg(OH)_2$ is a weakly basic, sparingly soluble compound with a solubility of approximately 6.4 mg/L
at room temperature, which corresponds to a theoretical pH of 10.34 in a saturated solution. In both RSS and CSS cases, the measured leachate pH remained below this theoretical value during the entire test period, indicating that the system did not reach a saturation state with respect to $Mg(OH)_2$. In leaching systems involving seawater, the major ionic species influencing leachate pH are Ca^{2+}, Mg^{2+}, and OH^-. These ions participate in competitive precipitation and buffering reactions, leading to a dynamic equilibrium that constrains further pH increase. The higher pH observed in the RSS case compared to the CSS case can be explained by the reduced availability of Ca^{2+} in the carbonated slag, as a significant portion of the calcium had already been stabilized as $CaCO_3$ during the CO_2 pressurized carbonation process. While the concentrations of Mg^{2+} introduced from seawater were consistent across both cases, the initial availability of Ca^{2+} and OH^- was lower in the CSS case, resulting in equilibrium being established at a comparatively lower pH.

Flow rate

The experimental design considered the possibility that faster flow might reduce the reaction time between the slag and liquid, thereby limiting the dissolution of Ca^{2+} and OH^- into the leachate. However, within the applied flow rates of 10 and 20 PV/hr, a clear difference in pH behavior was not observed. While a slightly lower pH was recorded at the higher flow rate. In Figs. 7(a)-7(b), the minor reduction of leachate pH was derived from fast flow rate conditions. Among all tested conditions, the greatest pH sensitivity to leaching volume was consistently observed in CDS and CDF cases (0.37 greater in the CDS case than in the CDF case).

This finding suggests that the washout effect due to faster flow rate has a greater effect than the injection fluid-

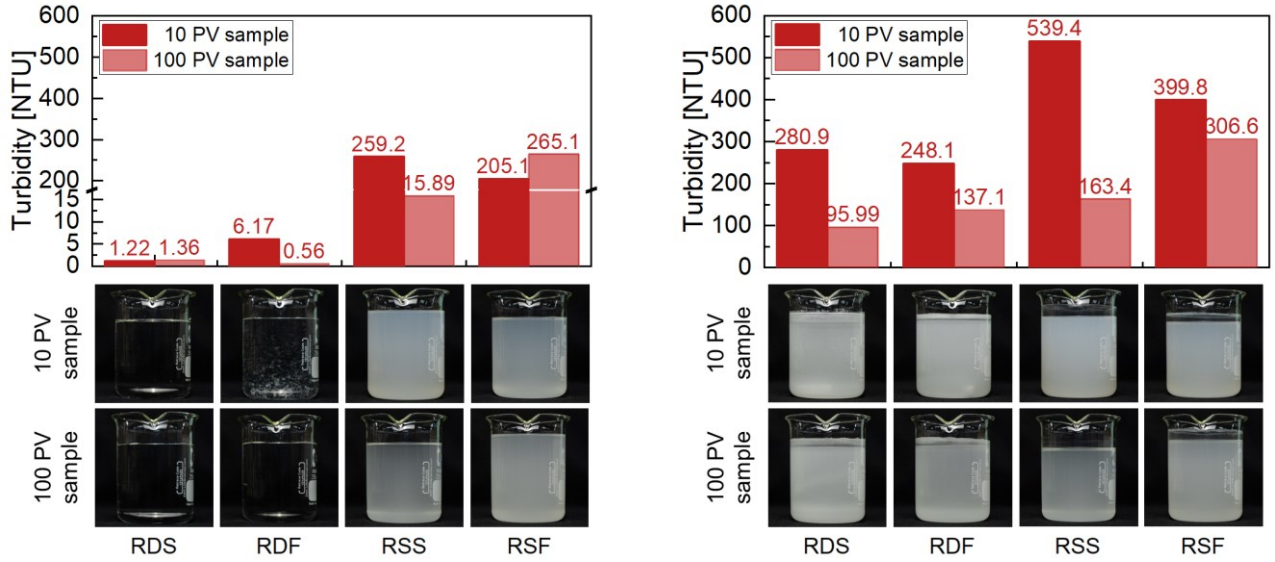

(a) Steel slag leachate samples immediately after sampling

(b) Steel slag leachate samples after accelerated 24-hour atmospheric exposure

Fig. 8 Turbidity and optical image of the leachate sample of BOF steel slag before CO_2 pressurization at 10 and 100 PV

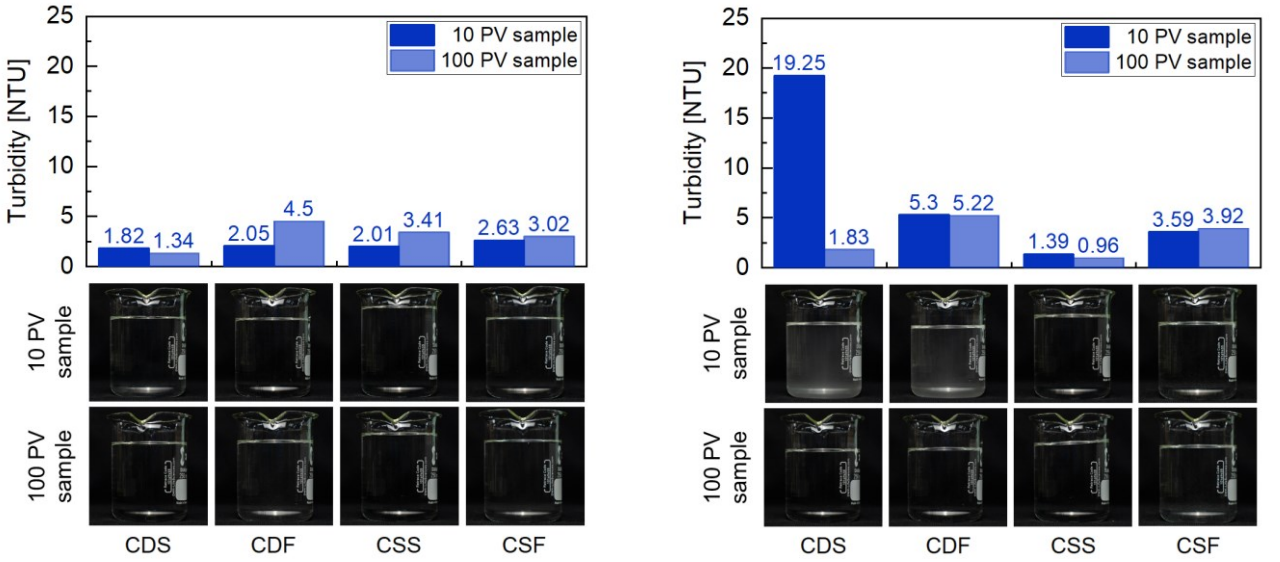

(a) Steel slag leachate samples immediately after sampling

(b) Steel slag leachate samples after accelerated 24-hour atmospheric exposure

Fig. 9 Turbidity and optical image of the leachate sample of CO_2 pressurized BOF steel slag at 10 and 100 PV

BOF steel slag reaction time, and also, it is shown to be weaker than the effects of CO_2 pressurized carbonation status and injected fluid type. In seawater injection cases, the system likely reached chemical equilibrium rapidly as seawater reacted with ions dissolved from the slag, due to the high and stable ionic concentrations in the inflow. In contrast, in distilled water injection, the leachate composition originated solely from dissolved constituents of BOF steel slag, which gradually diminished throughout leaching due to washout. For BOF steel slag before CO_2 pressurization, the concentration of OH^- ions released was sufficiently high that no substantial pH reduction was observed during the 100 PV leaching period. However, in CO_2 pressurized BOF steel slag, the residual CaO content was reduced, resulting in a lower OH^- release and a more pronounced pH decrease.

3.2.2 Turbidity of BOF steel slag leachate

The turbidity of BOF steel slag leachate was quantitatively analyzed in this study. In the leachate, Ca^{2+} ions react with carbonate ions (CO_3^{2-}) generated by the dissolution of atmospheric CO_2 to form $CaCO_3$ (Giacomin *et al*. 2020). The $CaCO_3$ formed through this reaction does not precipitate on the surface of the BOF steel slag but instead remains suspended in the leachate as fine particles, thereby causing turbidity. To accelerate this process,

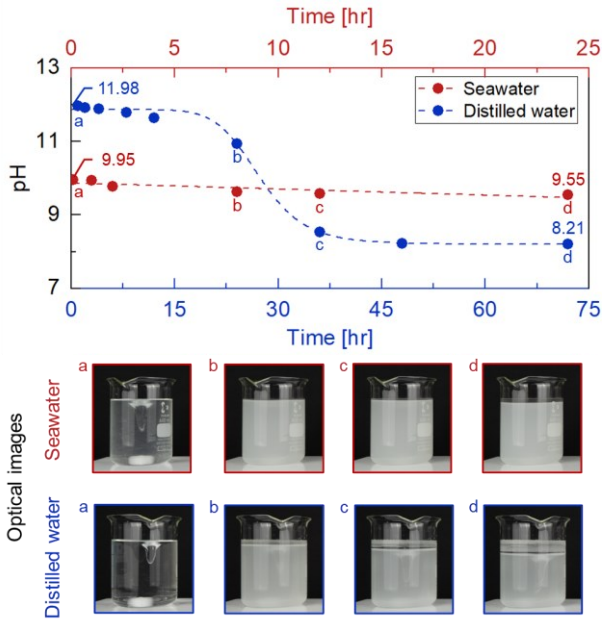

Fig. 10 pH evolution in accelerated atmospheric exposure after dissolving CaO in distilled water and seawater

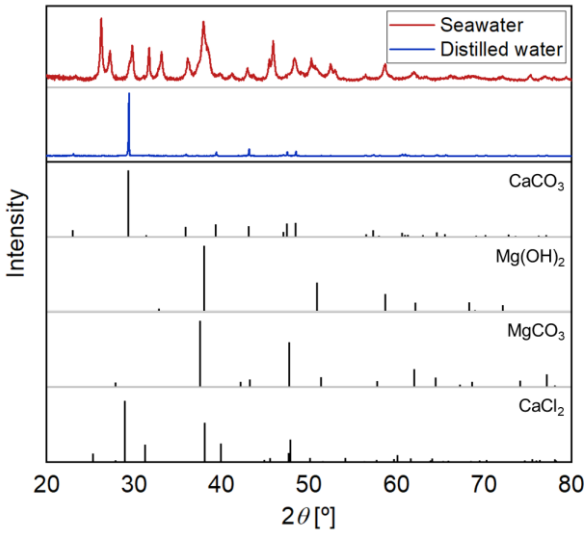

Fig. 11 XRD patterns of precipitates formed from CaO dissolved in distilled water and synthetic seawater after atmospheric exposure

leachate samples were subjected to continuous magnetic stirring at 700 rpm for 24 hours under 500 ppm CO_2 concentration atmospheric exposure. This section analyzes the mechanisms responsible for turbidity formation in steel slag leachate and investigates the effect of CO_2 pressurized carbonation in reducing the generation of suspended fines.

Injected fluid type

The use of seawater as the injecting fluid resulted in the formation of salts through multiple ionic reactions, producing higher turbidity than that observed with distilled water. Fig. 8(a) shows the turbidity of leachate samples collected from BOF steel slag before CO_2 pressurization at 10 and 100 PV, measured immediately after sampling. To ensure visual consistency, all sample images were taken under identical lighting and camera settings (white balance: 6,300 K, aperture: f/8, shutter speed: 1/60 sec, ISO: 1,250). In Figs. 8(a)-8(b), turbidity at 10 PV is represented by vivid red columns and at 100 PV by pale red columns. In the distilled water injected cases (RDS and RDF), the turbidity remained consistently below 10 NTU. The RDF case at 10 PV showed the highest value at 6.17 NTU, likely due to the presence of suspended fines, while the remaining samples (RDF-100 PV, RDS) showed values between 0.56 and 1.36 NTU. The seawater injected samples exhibited much higher turbidity. This was particularly notable in the RSS case, where turbidity decreased from 259.2 NTU at 10 PV to 15.89 NTU at 100 PV. However, in the RSF case, turbidity increased over time, from 205.1 NTU at 10 PV to 265.1 NTU at 100 PV. Compared to the CDS and CDF cases in Fig. 9(a), turbidity remained low regardless of carbonation status in the distilled water injected cases. In contrast, turbidity in seawater injected cases was consistently higher, often exceeding 200 NTU. This indicates that the reaction between Mg^{2+} and OH^-, which forms $Mg(OH)_2$, occurs more rapidly than the slower process of $CaCO_3$ formation via atmospheric CO_2 dissolution and carbonate ion generation, resulting in high turbidity even immediately after sampling.

Fig. 8(b) illustrates turbidity measurements after a 24-hour accelerated reaction with atmospheric CO_2. Turbidity increased in all cases following CO_2 exposure. For instance, the 100 PV RDS sample increased from an initial 1.36 NTU to 95.99 NTU, demonstrating significant $CaCO_3$ precipitation, also clearly visible in the sample image. The highest turbidity after CO_2 exposure was observed in the RSS case at 10 PV, reaching 539.4 NTU. Across all conditions, turbidity at 100 PV was lower than at 10 PV, regardless of flow rate or liquid type. This can be explained by the progressive washout of reactive calcium from the slag during leaching. After CO_2 exposure, dissolved CO_2 forms carbonate ions that react with Ca^{2+} and Mg^{2+} to form $CaCO_3$ and $MgCO_3$, increasing suspended solids.

The turbidity difference caused by the type of injected fluid is associated with the formation of poorly soluble salts such as $Mg(OH)_2$ and $CaCl_2$. These salts are generated through reactions between Mg^{2+} and Cl^- ions from seawater and Ca^{2+} and OH^- ions released from the slag, resulting in visible suspended precipitates (Zhang *et al.* 2012). Neutralization reactions involving H^+ and OH^- ions contribute to pH stabilization. Immediately after sampling, the turbidity trend with leaching volume was less consistent due to the presence of slag-derived fines. However, after CO_2 exposure, carbonate precipitation became the dominant mechanism contributing to turbidity. The lower turbidity observed in later-stage samples reflects a reduction in available Ca^{2+} due to prior leaching.

CO_2 pressurized carbonation status

CO_2 pressurization suppressed the potential formation of turbidity in BOF steel slag through the crystallization of CaO into $CaCO_3$. Fig. 9(a) presents the turbidity of leachate samples collected at 10 PV (vivid blue columns) and 100 PV (pale blue columns) from CO_2 pressurized BOF steel

slag injected with either distilled water or seawater, measured immediately after sampling. Comparing distilled water injected cases in Fig. 8(a) (RDS, RDF vs. CDS, CDF), the measured turbidity ranged from 1.22–6.17 NTU for leachate of BOF steel slag before CO_2 pressurization and 1.34–4.50 NTU for leachate of CO_2 pressurized carbonated slag, indicating no significant difference due to CO_2 pressurization. The highest turbidity was observed in the CDF case at 100 PV (4.50 NTU), but this still falls within the low turbidity range observed across distilled water cases. For seawater injection, the effect of carbonation was much more pronounced. In RSS and RSF cases, turbidity ranged from 15.89–265.1 NTU, significantly higher than in distilled water injected cases. In CSS and CSF cases, turbidity was limited to 2.01–3.41 NTU, similar to the distilled water injected cases. This contrast indicates that carbonation effectively reduced the availability of free-CaO in BOF steel slag, thereby suppressing reactions with seawater ions (Mg^{2+}, Cl^-) that would otherwise form additional precipitates such as $Mg(OH)_2$ and $CaCl_2$.

Fig. 9(b) shows the turbidity of the same leachate samples after 24 hours of accelerated exposure to atmospheric CO_2. Under these conditions, residual Ca^{2+} and Mg^{2+} in the leachate reacted with dissolved CO_2 to form $CaCO_3$ and $MgCO_3$, resulting in increased turbidity in most cases. Among the CO_2 pressurized BOF steel slag cases, 3 out of 4 exhibited increased turbidity after CO_2 exposure, with values ranging from 0.96-19.25 NTU. The CSS case showed a slight decrease, but given the low absolute values involved (<3.41 NTU), this is considered to fall within the range of measurement uncertainty. In comparison, samples of BOF steel slag before CO_2 pressurization subjected to the same atmospheric exposure (Fig. 8(b)) exhibited a much larger turbidity increase, ranging from 95.99–539.4 NTU. Specifically, turbidity increased by 41.5–280.2 NTU in raw slag, whereas in CO_2 pressurized carbonated slag, the increase was limited to just 0.49–17.43 NTU. This substantial suppression of turbidity in the carbonated samples confirms the effectiveness of CO_2 pressurized carbonation in mineralizing CaO into $CaCO_3$, thereby reducing the availability of reactive calcium in leachate.

4. Discussions

To further clarify the origin of turbidity and pH reduction observed in the steel slag leachate, a controlled experiment was conducted using pure CaO reagent dissolved in distilled water and synthetic seawater, followed by atmospheric exposure. This test aimed to isolate the chemical reactions responsible for turbidity generation, specifically those attributed to the CaO component in the slag. Fig. 10 shows the evolution of pH and qualitative turbidity over time. In the distilled water case (blue circles with dashed line), CaO was dissolved at a concentration of 0.2618 g/L and allowed to react with atmospheric CO_2 for 72 hours. The initial pH of 11.98 decreased to 8.21 within this period and then stabilized. Turbidity was visually observed to increase over time, indicating progressive precipitation of carbonate species. In contrast, when CaO was dissolved in synthetic seawater (red circles with dashed line), the initial pH was lower (9.95), due to buffering effects from Mg^{2+} and other ions present in the seawater matrix. Turbidity developed rapidly even at the earliest time points, and pH dropped by 0.4 units within the 24 hours of reaction.

Fig. 11 presents the X-Ray Diffraction (XRD) patterns of the precipitates formed in each solution after atmospheric exposure. In the distilled water case (blue line), only $CaCO_3$ peak patterns were observed, indicating a single-phase carbonate formation. In the seawater case (red line), additional diffraction peaks corresponding to $Mg(OH)_2$, $MgCO_3$, and $CaCl_2$ were detected, along with $CaCO_3$. The reference patterns from the International Centre for Diffraction Data (ICDD) are included for comparison. These results confirm that in seawater environments, multiple minerals can form due to interactions between Ca^{2+} released from CaO and seawater ions such as Mg^{2+} and Cl^-.

These findings provide direct evidence that the turbidity observed in the steel slag leachate, especially when infiltrated by seawater, is primarily the result of precipitation reactions involving residual CaO and seawater constituents. The suppression of such turbidity in carbonated slag, as observed in Section 3.4, can thus be attributed to prior mineralization of CaO into $CaCO_3$ through CO_2 pressurized carbonation.

5. Conclusions

This study investigated the characteristics of BOF steel slag leachate, focusing on the chemical mechanisms that lead to undesirable leachate properties such as high alkalinity and turbidity. A series of continuous leaching experiments and mineralogical analyses concluded the following salient observations:

• Calcium in BOF steel slag exists in various chemical forms, including CaO, $Ca(OH)_2$, and C_2S. When present as CaO or $Ca(OH)_2$, these compounds react readily with water, releasing OH^- ions and creating a strongly alkaline environment. Calcium in its ionic form (Ca^{2+}) can also react with atmospheric CO_2, forming $CaCO_3$ as suspended fines in the leachate, and this is a potential source of turbidity. Such reactions may occur during stockyard aging or in situ conditions when slag is used as a fill material and exposed to rainfall or groundwater.

• CO_2 pressurized carbonation of BOF steel slag can preemptively mineralize reactive calcium into $CaCO_3$, thereby reducing the potential for subsequent ion dissolution and leaching. However, since this process requires dedicated pressurization equipment, its field-scale application would necessitate further evaluation of economic feasibility.

• Seawater treatment offers a practical and cost-effective method for reducing the alkalinity of BOF steel slag leachate. Given that most steelworks are located along coastlines, seawater is a readily available resource. Pre-treatment with seawater before open-air aging could limit the migration of alkaline species and turbidity-causing fines

into the surrounding environment during rainfall or water spray operations. Unlike CO_2 pressurized carbonation, this approach does not require pressure equipment. Moreover, combining CO_2 pressurization with seawater treatment may yield synergistic effects, further enhancing pH stabilization and suppressing the formation of suspended fines.

• The effects of injected fluid volume and flow rate on leachate pH were found to be minor. The minimal impact suggests that the reaction between the fluid and the slag occurs rapidly and is largely insensitive to residence time. This indicates that seawater pre-treatment, if applied, does not require prolonged contact durations or large water volumes, thus offering practical advantages for on-site implementation.

By understanding and controlling the reactions that occur during contact with water and atmospheric CO_2, this study provides a basis for more predictable and responsible slag management strategies in civil engineering applications. Moreover, the carbonation of steel slag is a mineral carbonation process in which CaO reacts with CO_2 to form $CaCO_3$. The resulting $CaCO_3$ is a thermodynamically stable mineral that does not readily decompose under ordinary environmental conditions (Karunadasa *et al*. 2019). Unless subjected to highly acidic solutions or temperatures above approximately 550 °C, it remains intact. Therefore, pressurized carbonation of BOF steel slag can offer a semi-permanent solution for CO_2 sequestration while also mitigating issues related to high pH and turbidity in leachate (Kim *et al*. 2020).

Acknowledgments

This work was supported by the National Research Foundation of Korea (NRF) grant funded by the Korean government (MSIT) (No. RS-2021-NR060085).

References

Baalamurugan, J., Kumar, V.G., Padmapriya, R. and Raja, V.B. (2024). "Recent applications of steel slag in construction industry", *Environ. Develop. Sustain.*, **26**(2), 2865-2896. https://doi.org/10.1007/s10668-022-02894-3.

Bertos, M.F., Li, X., Simons, S.J.R., Hills, C.D. and Carey, P.J. (2004), "Investigation of accelerated carbonation for the stabilisation of MSW incinerator ashes and the sequestration of CO_2", *Green Chemistry*, **6**(8), 428-436. https://doi.org/10.1039/B401872A.

Blue, C.R., Giuffre, A., Mergelsberg, S., Han, N., De Yoreo, J.J. and Dove, P.M. (2017), "Chemical and physical controls on the transformation of amorphous calcium carbonate into crystalline $CaCO_3$ polymorphs", *Geochimica et Cosmochimica Acta*, **196**, 179-196. https://doi.org/10.1016/j.gca.2016.09.004.

Bychkov, A.Y., Bénézeth, P., Pokrovsky, O.S., Shvarov, Y.V., Castillo, A. and Schott, J. (2020), "Experimental determination of calcite solubility and the stability of aqueous Ca–and Na–carbonate and–bicarbonate complexes at 100–160° C and 1–50 bar pCO2 using in situ pH measurements", *Geochimica et Cosmochimica Acta*, **290**, 352-365. https://doi.org/10.1016/j.gca.2020.09.004.

Coats, A.W. and Redfern, J.P. (1963), "Thermogravimetric analysis. A review", *Analyst*, **88**(1053), 906-924. https://doi.org/10.1039/AN9638800906.

Engström, F., Larsson, M.L., Samuelsson, C., Sandström, Å., Robinson, R. and Björkman, B. (2014), "Leaching behavior of aged steel slags", *Steel Res. Int.*, **85**(4), 607-615. https://doi.org/10.1002/srin.201300119.

Euroslag (2018), The European Association representing metallurgical slag producers and processors; DOWNLOADS; Statistical Data. https://www.euroslag.com/research-library-downloads/downloads/ (Accessed Statistics 2018).

Fitzgerald, R., Keil, K. and Heinrich, K.F. (1968), "Solid-state energy-dispersion spectrometer for electron-microprobe X-ray analysis", *Science*, **159**(3814), 528-530. https://doi.org/10.1126/science.159.3814.528.

Galan, I., Glasser, F.P. and Andrade, C. (2013), "Calcium carbonate decomposition", *J. Thermal Anal. Calorimetry*, **111**, 1197-1202. https://doi.org/10.1007/s10973-012-2290-x.

Giacomin, C. E., Holm, T., & Mérida, W. (2020). "$CaCO_3$ growth in conditions used for direct air capture". *Powder Technology*, **370**, 39-47. https://doi.org/10.1016/j.powtec.2020.05.018.

Gunning, P.J., Hills, C.D. and Carey, P.J. (2010), "Accelerated carbonation treatment of industrial wastes", *Waste Manage.*, **30**(6), 1081-1090. https://doi.org/10.1016/j.wasman.2010.01.005.

Huijgen, W.J. and Comans, R.N. (2006), "Carbonation of steel slag for CO_2 sequestration: leaching of products and reaction mechanisms", *Environ. Sci. Technol.*, **40**(8), 2790-2796. https://doi.org/10.1021/es052534b.

Huijgen, W.J., Witkamp, G.J. and Comans, R.N. (2005), "Mineral CO_2 sequestration by steel slag carbonation", *Environ. Sci. Technol.*, **39**(24), 9676-9682. https://doi.org/10.1021/es050795f.

Karunadasa, K.S., Manoratne, C.H., Pitawala, H.M.T.G.A. and Rajapakse, R.M.G. (2019), "Thermal decomposition of calcium carbonate (calcite polymorph) as examined by in-situ high-temperature X-ray powder diffraction", *J. Phys. Chemistry Solids*, **134**, 21-28. https://doi.org/10.1016/j.jpcs.2019.05.023.

Kilic, S., Toprak, G. and Ozdemir, E. (2016), "Stability of $CaCO_3$ in $Ca(OH)_2$ solution", *Int. J. Mineral Processing*, **147**, 1-9. https://doi.org/10.1016/j.minpro.2015.12.006.

Kim, S.H., Jeong, S., Chung, H. and Nam, K. (2020), "Mechanism for alkaline leachate reduction through calcium carbonate precipitation on basic oxygen furnace slag by different carbonate sources: application of $NaHCO_3$ and CO_2 gas", *Waste Manage.*, **103**, 122-127. https://doi.org/10.1016/j.wasman.2019.12.019.

Korea Iron & Steel Association (2024), *Korea Iron & Steel Association*, *2024*. Information Center; Data Room. https://www.kosa.or.kr/ (Accessed Promotional Brochure for Steel Slag 2024).

Korea Iron & Steel Association (2024), *Korea Iron & Steel Association, 2024*. Information Center; Data Room. https://www.kosa.or.kr/ (Environmental Safety Assessment of Steel Slag).

Li, H., Tang, Z., Li, N., Cui, L. and Mao, X.Z. (2020), "Mechanism and process study on steel slag enhancement for CO_2 capture by seawater", *Appl. Energy*, **276**, 115515. https://doi.org/10.1016/j.apenergy.2020.115515.

Liu, L., Liu, L., Liu, Z., Yang, C., Li, X. and Huang, Y. (2024), "Effects of the Aging Treatment Process on the Properties of Steel Slag", *J. Mater. Civil Eng.*, **36**(4), 04024019. https://doi.org/10.1061/JMCEE7.MTENG-16508.

Ma, J., Kim, D., Kim, S., Byun, Y.H. and Yun, T.S. (2024), "Conversion efficiency of carbonate formation from steel slag via CO_2 pressurization", *Steel Compos. Struct.*, **53**(5), 575-587. https://doi.org/10.12989/scs.2024.53.5.575.

Moon, H.Y., Yoo, J.H. and Kim, S.S. (2002), "A fundamental study on the steel slag aggregate for concrete", *Geosystem Eng.*, **5**(2), 38-45. https://doi.org/10.1080/12269328.2002.10541186.

Nancollas, G.H. and Reddy, M.M. (1971), "The crystallization of calcium carbonate. II. Calcite growth mechanism", *J. Colloid Interface Sci.*, **37**(4), 824-830. https://doi.org/10.1016/0021-9797(71)90363-8.

O'Connor, J., Nguyen, T.B.T., Honeyands, T., Monaghan, B., O'Dea, D., Rinklebe, J. and Bolan, N. (2021), "Production, characterisation, utilisation, and beneficial soil application of steel slag: A review", *J. Hazard. Mater.*, **419**, 126478. https://doi.org/10.1016/j.jhazmat.2021.126478.

Pan, S.Y., Chung, T.C., Ho, C.C., Hou, C.J., Chen, Y.H. and Chiang, P.C. (2017), "CO_2 mineralization and utilization using steel slag for establishing a waste-to-resource supply chain", *Sci. Reports*, **7**(1), 17227. https://doi.org/10.1038/s41598-017-17648-9.

Spínola, A.C., Pinheiro, C.T., Ferreira, A.G. and Gando-Ferreira, L. M. (2021), "Mineral carbonation of a pulp and paper industry waste for CO_2 sequestration", *Process Safety Environ. Protect.*, **148**, 968-979. https://doi.org/10.1016/j.psep.2021.02.019.

US Geological Survey (2025), *US Geological Survey, 2025. Mineral Commodity Summaries: Slag-Iron and Steel; U.S. Geological Survey*, Washington, DC, US. https://www.usgs.gov/centers/national-minerals-information-center/iron-and-steel-slag-statistics-and-information?qt-science_support_page_related_con=0#qt-science_support_page_related_con

Wang, L., Chen, L., Tsang, D.C., Li, J.S., Yeung, T.L., Ding, S. and Poon, C.S. (2018), "Green remediation of contaminated sediment by stabilization/solidification with industrial by-products and CO_2 utilization", *Sci. Total Environ.*, **631**, 1321-1327. https://doi.org/10.1016/j.scitotenv.2018.03.103.

Wang, M., Wang, X., Zhang, M., Han, W., Yuan, Z., Zhong, X. and Ji, H. (2023), "Treatment of Cd (II) and As (V) co-contamination in aqueous environment by steel slag-biochar composites and its mechanism", *J. Hazard. Mater.*, **447**, 130784. https://doi.org/10.1016/j.jhazmat.2023.130784.

Wang, Q., Yan, P., Yang, J. and Zhang, B. (2013), "Influence of steel slag on mechanical properties and durability of concrete", *Construct. Build. Mater.*, **47**, 1414-1420. https://doi.org/10.1016/j.conbuildmat.2013.06.044.

Zhang, X., Matsuura, H. and Tsukihashi, F. (2012), "Dissolution mechanism of various elements into seawater for recycling of steelmaking slag", *ISIJ Int.*, **52**(5), 928-933. https://doi.org/10.2355/isijinternational.52.928.